UC Irvine
UC Irvine Previously Published Works

Title
Hindered cytoplasmic diffusion of inositol trisphosphate restricts its cellular range of action

Permalink
https://escholarship.org/uc/item/9jm388mz

Journal
Science Signaling, 9(453)

ISSN
1945-0877

Authors
Dickinson, George D
Ellefsen, Kyle L
Dawson, Silvina Ponce
et al.

Publication Date
2016-11-08

DOI
10.1126/scisignal.aag1625

Peer reviewed

eScholarship.org Powered by the California Digital Library
University of California

Author Manuscript

Author Manuscript

Author Manuscript

Author Manuscript

HHS Public Access

Author manuscript

Sci Signal. Author manuscript; available in PMC 2017 July 19.

Published in final edited form as:

Sci Signal. ; 9(453): ra108. doi:10.1126/scisignal.aag1625.

Hindered cytoplasmic diffusion of inositol trisphosphate restricts its cellular range of action

George D. Dickinson[1], **Kyle L. Ellefsen**[1], **Silvina Ponce Dawson**[2], **John E. Pearson**[3], and **Ian Parker**[1,4]

[1]Department of Neurobiology & Behavior, University of California, Irvine, CA92697, USA

[2]Departamento de Física, FCEN-UBA and IFIBA, CONICET, Buenos Aires, Argentina

[3]Theoretical Biology & Biophysics, T-10 MS K710, Los Alamos National Laboratory, Los Alamos, NM, 87545 USA

[4]Department of Physiology & Biophysics, University of California, Irvine, CA92697, USA

Abstract

The range of action of intracellular messengers is determined by their rates of diffusion and degradation. Previous measurements in oocyte cytoplasmic extracts indicated that the Ca^{2+}-liberating second messenger inositol trisphosphate (IP_3) diffuses with a coefficient (~280 $\mu m^2\ s^{-1}$) similar to that in water, corresponding to a range of action of ~25 μm. Consequently, IP_3 is generally considered a 'global' cellular messenger. We re-examined this issue by measuring local IP_3-evoked Ca^{2+} puffs to monitor IP_3 diffusing from spot photorelease in neuroblastoma cells. Fitting these data by numerical simulations yielded a diffusion coefficient (≤10 $\mu m^2\ s^{-1}$) about 30 fold slower than previously reported. We propose that diffusion of IP_3 in mammalian cells is hindered by binding to immobile, functionally inactive receptors that were diluted in oocyte extracts. The predicted range of action of IP_3 (<5 μm) is thus smaller than the size of typical mammalian cells, indicating that IP_3 should better be considered as a local rather than global cellular messenger.

Correspondence should be sent to: Dr. George Dickinson, Address: 1146 McGaugh Hall, Department of Neurobiology & Behavior, University of California, Irvine, CA 92697, Phone: (949)-824-7833: Fax: (949)-824-2447, dickinsg@uci.edu.

SUPPLEMENTARY MATERIALS

Methods S1. Theoretical derivation of puff latencies

Methods S2. Calculation of range of action

Fig. S2. Ca^{2+} waves evoked by photoreleased i-IP_3 in SH-SY5Y cells without EGTA.

Fig. S3. Latencies of puffs evoked by spot photorelease of i-IP_3 in COS-7 cells.

Fig. S4. Lengths of SH-SY5Y cells and spatial extent of the photolysis laser spot

Fig. S5. Experimental and simulated first-puff latency data for 100 and 200 ms spot flash durations

References (37)

Movie M1. Puffs evoked by localized and distributed flash photorelease of IP_3

Author contributions: G.D.D. performed experiments and analyzed experimental data. K.L.E. wrote analytical and simulation software and together with G.D.D. performed numerical simulations. J.E.P. & S.P.D. formulated the analytical solutions and performed statistical analysis. I.P. conceived and supervised the project. All authors contributed to writing the paper, and read and approved the final manuscript.

Competing interests: The authors declare no competing interests.

Data and software availability: Raw data and custom software are freely available to academic researchers on request.

Author Manuscript Author Manuscript Author Manuscript Author Manuscript

INTRODUCTION

In a classic paper, Allbritton *et al.* (1) introduced the concept of the 'range of action' of an intracellular messenger, specifically considering the distance from a source over which Ca^{2+} ions and inositol trisphosphate (IP_3) can exert their actions. The range of action is determined by how far a messenger can diffuse, on average, before it is removed from the cytosol by degradation (IP_3) or sequestration (Ca^{2+}). To experimentally determine diffusion rates, Allbritton *et al.* (1) prepared slabs of cytosolic extract from *Xenopus* oocytes, and measured the penetration over time of radiolabelled Ca^{2+} and IP_3 presented to one side of a slab after inhibiting degradation and sequestration mechanisms. The apparent diffusion coefficient they obtained for IP_3 ($283 \pm 53\ \mu m^2\ s^{-1}$) was similar to that expected for free diffusion in a medium with twice the viscosity of water, whereas the value for Ca^{2+} was much lower ($38 \pm 11\ \mu m^2\ s^{-1}$), concordant with hindered diffusion in the presence of immobile Ca^{2+}-binding buffers. Taking into account the respective rates of degradation and sequestration of IP_3 and Ca^{2+}, Sims & Allbritton (2) concluded that Ca^{2+} has a narrow cytosolic range of action and serves as a local signal, whereas IP_3 functions as a global signal because its range of action is greater than the dimensions of typical mammalian cells.

Here, we reconsider the issue of diffusion of IP_3 in the cytosol in light of observations suggesting that binding to immobile sites may appreciably slow the effective diffusion of IP_3 in mammalian cells. In SH-SY5Y neuroblastoma cells and other cell lines IP_3 primarily evokes Ca^{2+} release from only a few hundred functional IP_3 receptors (IP_3Rs), clustered at discrete sites (3, 4). Different from this, immunostaining of IP_3Rs reveals a dense distribution throughout the cell, and radioligand assays indicate the presence of about 30,000 IP_3R monomers (IP_3 binding sites) per cell (5–8). If these functionally 'silent' IP_3Rs bind IP_3, they would hinder its diffusion without contributing to the Ca^{2+} signal.

We thus set out to determine the effective diffusion coefficient of IP_3 in intact mammalian cells. We uniformly loaded SH-SY5Y cells with a caged, poorly-metabolized IP_3 analog (i-IP_3) and selectively photoreleased i-IP_3 using flash photolysis by a UV laser spot positioned at one end of these elongated cells. This increased the cytosolic concentration of i-IP_3 at the location of the laser spot, which subsequently equilibrated throughout the cell as free i-IP_3 diffused from the site of origin. To monitor the spread of i-IP_3, we utilized IP_3-evoked Ca^{2+} liberation (Ca^{2+} puffs) from local clusters of IP_3Rs (4, 9) as endogenous and sensitive detectors that are distributed throughout the cell. As previously reported (10), control experiments in which i-IP_3 was uniformly photoreleased across a cell showed that the mean latency between photorelease and the occurrence of the first puff at a site shortened in about linear proportion with increasing concentration of i-IP_3 whereas the latency did not vary systematically along the length of the cell. Thus, we could use the mean puff latency at sites at different distances from the laser spot as a measure of the temporal profile of the concentration of i-IP_3 ([i-IP_3]) at those locations. If i-IP_3 were to diffuse sufficiently rapidly that its concentration neared equilibrium within the mean first-puff latency, then we would expect similar latencies at all locations. Instead, we observed that mean first-puff latencies were as much as 20 times longer at the distal end of cells as compared to sites proximate to the UV spot. By comparing these data to model predictions, we derive an estimate for the effective diffusion coefficient of IP_3 in the cytosol of 5–10 $\mu m^2\ s^{-1}$; about 30 fold lower than

Author Manuscript Author Manuscript Author Manuscript Author Manuscript

the widely accepted value obtained by Allbritton *et al.* (1). We thus propose that IP_3 is better considered as a local, rather than global, messenger in mammalian cells.

RESULTS

Puffs evoked by localized and distributed photorelease of i-IP_3

We loaded SH-SY5Y cells with the Ca^{2+} indicator Fluo-4 and a caged precursor of i-IP_3, an analog of IP_3 that is slowly metabolized (11) and evokes Ca^{2+} puffs (puffs) that persist in the cells following flash photorelease with little diminution in mean frequency for more than two minutes (3, 4, 12). During the time course of recordings (30 s), we thus assumed that degradation of i-IP_3 was negligible, so that the total amount that was photoreleased could be assumed to remain constant. Moreover, the latencies of puffs evoked by a given, spatially uniform photolysis flash showed only small variation between different cells (standard deviation 40% of mean; 24 cells), indicating a relatively consistent loading of caged i-IP_3. We also loaded the cells with the slow Ca^{2+} buffer EGTA to suppress global Ca^{2+} waves that could be triggered by the released Ca^{2+} (13). Localized, transient Ca^{2+} puffs were evoked by photoreleasing i-IP_3 using a focused laser spot of 405 nm light that was either stationary and positioned so that it illuminated within one end of a cell (spot flash) or was rapidly and uniformly stepped across the length of the cell (distributed flash) (Fig. 1A). In both cases the intensity and total duration of the laser flash were identical, delivering the same number of photons, and hence photoreleasing the same average amount of i-IP_3. However, because of the difference in spatial profile of the photoreleased i-IP_3, we expected that the spot flash stimulation would evoke puffs beginning, on average, after longer latencies at greater distances from the spot because of the time scale and dilution imposed if i-IP_3 were to diffuse slowly, whereas the distributed flash stimulation would result in a rapid and near homogeneous increase in [i-IP_3] throughout the cell.

We mapped the locations of puffs evoked by photoreleased IP_3 throughout a 30s recording (Fig. 1B), and monitored fluorescence ratio traces ($\Delta F/F_0$) from regions of interest centered on these sites (Fig. 1C). We measured the latency to the first puff at each site as a function of the distance of the site from spot flash (Fig. 1D, upper panel) or to the lower end of cells receiving distributed flash stimulation (Fig. 1D, lower panel). Although there was considerable scatter in the data, these plots showed that puff latencies were longer at sites more distant from the stationary laser spot, whereas there was no obvious systematic variation of puff latency with position along the cell in the case of the distributed stimulation.

Determination of mean first-puff latencies

Puffs are stochastic events, and their latencies following spatially uniform photorelease of a given amount of IP_3 are exponentially distributed (9, 10). To obtain estimates of mean latencies by pooling data from multiple puff sites in many cells, we automated the detection and localization of puffs using a freely-available, custom software algorithm (14). This algorithm reported the latency of each event from the beginning of the photolysis flash together with the distance from the centroid locations of a puff in relation to the spot flash or, arbitrarily, to one end of the cell in trials with distributed flash stimulation. Trials with

Author Manuscript Author Manuscript Author Manuscript Author Manuscript

spot flash and distributed flash stimulation were performed in alternating order, using a constant intensity and differing total flash durations (100, 200, and 500 ms).

Individual first-puff latencies evoked by spot flash of i-IP_3 with flash durations of 100, 200, or 500 ms showed considerable variability (Fig. 2A), as expected, but mean latencies calculated by binning the data points over approximately 5 μm increments revealed a dependence on distance from the site of photorelease for all three flash durations (Fig. 2B). Mean puff latencies at sites near the laser spot were shorter for longer flash durations but lengthened to ~10s for all flash durations at the end of the cell farthest from the spot flash stimulation site. In contrast, distributed flash stimulation of i-IP_3 throughout the cell evoked puffs with latencies that lacked a systematic relationship with location along the cell but, on average, shortened progressively with increasing flash duration (Figs. 2C, D). To further validate the difference in spatial distribution of first-puff latencies between the spot flash and distributed photorelease of i-IP_3, we performed a linear regression to fit a linear function of the distance along the cell to the logarithm of the individual first-puff latencies as plotted in Figs. 2A,C. Latencies depended strongly on distance from the spot flash stimulation for all flash durations, as manifest by slopes differing significantly from zero, whereas there was no significant distance-dependence for distributed flash stimulation (Fig. S1).

These experiments to determine puff latencies were necessarily performed with cells loaded with EGTA to suppress global Ca^{2+} waves. To verify that the stimulation conditions produced physiologically relevant IP_3 concentrations, we photoreleased equivalent amounts of i-IP_3 in cells that had not been loaded with EGTA (Fig. S2). We observed global Ca^{2+} signals in 13/16 (81%) cells stimulated with a 100 ms duration distributed flash stimulation; in 16/21 (76%) cells with a 200 ms flash; and 19/19 (100%) cells with a 500 ms flash. In parallel experiments in EGTA-loaded cells the 200 ms flash evoked puffs with a mean latency of 6.3 s, closely matching that in the experiment of Fig. 2D. Therefore, the stimulus conditions were in a physiologically relevant range of IP_3 concentrations.

The data shown for the SH-SY5Y cells were obtained using the same culture of cells loaded under the same conditions to ensure internal consistency. We observed similar results in two other experiments with SH-SY5Y cells and one with COS-7 cells in which we measured 17 cells (Fig. S3A, B).

The overall mean latencies of puffs evoked by distributed flash stimulation decreased as the duration of the flash and, for each given flash duration, the distributions of puff latencies approximated exponential functions (Fig. 3A), consistent with previous findings (10). In contrast to the lack of spatial variation in puff latencies following distributed flash stimulation, the latency distributions of puffs evoked by a 500 ms spot flash stimulation varied with distance, with a time constant of ~1 s within <15 μm of the spot and ~10 s at sites >15 μm away (Fig. 3B).

Given that the latency to first occurrence of a puff at a site is an inverse function of [IP_3] (10), we interpreted the increasing first-puff latency at greater distances from the spot flash stimulation to arise from the time needed for i-IP_3 to diffuse along the length of the cell. To derive the diffusion rate of i-IP_3 in the cytosol, we needed to know how the latency varies

Author Manuscript Author Manuscript Author Manuscript Author Manuscript

with flash duration (amount of photoreleased i-IP_3) under our experimental conditions. To obtain this relationship, we plotted (Fig. 3C) the mean latencies of first-puffs evoked by distributed flash stimulation as a function of reciprocal flash duration; a linearly proportional measure of the amount of photoreleased i-IP_3, assuming that only a small fraction of the caged i-IP_3 was photolysed (15). Concordant with previous findings (10), the data fit to a linear relationship with the latency shortening in direct proportion to increasing [i-IP_3]. The slope of the relationship (0.90 ± 0.05 in units relative to flash duration) then allowed us to construct a model of the predicted distribution of puff latencies as i-IP_3 diffused through the cell.

Simulation of IP_3 diffusion and puff triggering

To obtain a quantitative estimate of the effective diffusion coefficient of IP_3, we compared our experimental data of first-puff latencies with predictions obtained by model simulations of the diffusion equation using various diffusion coefficients (methods S1: Theoretical derivation of puff latencies). We used a simplified, closed-end, one-dimensional model, representing the average length of cells used in the experiments (40 μm, Fig. S4A). In the model, we introduced IP_3 at the site of spot flash stimulation in relative amounts corresponding to the different flash durations, over a time course matching the flash duration and with a spatial distribution approximating that of the UV laser spot (fig. S4B). Following introduction of IP_3, we assumed that the total amount remained constant, mimicking the slow degradation of i-IP_3 in the cytosol (3, 4).

Heat maps of simulated spatiotemporal profiles of IP_3 concentration resulting from a modeled 500 ms flash illustrate the different results obtained with two effective diffusion coefficients: 10 $\mu m^2 s^{-1}$ (Fig. 4A) and 280 $\mu m^2 s^{-1}$, the value obtained by Allbritton *et al.* (1) (Fig. 4B). From these simulation results, we plotted the change in IP_3 concentrations over time at selected distances along the modeled cells with the different diffusion constants (Fig. 4C, D). When the diffusion coefficient was set to 280 $\mu m^2 s^{-1}$, the IP_3 concentration equilibrated across the cell within about 1 s to a final normalized concentration of ~0.11. For a diffusion coefficient of 10 $\mu m^2 s^{-1}$, the local concentration of IP_3 in the vicinity of the modeled spot flash remained considerably greater than the final equilibrium concentration for several seconds, whereas the concentration at the distal end of the cell did not begin to increase appreciably for more than 5 s and was still below the equilibrium level after as long as 20 s.

We used these predicted spatiotemporal concentration profiles to compute the probability of observing a puff at each position along the length of the one-dimensional cell at any given time following the introduction of IP_3 (onset of the spot flash, methods S1). For each spatial element and time point in the model, we calculated the puff-triggering rate that corresponded to the instantaneous concentration of IP_3 predicted by the simulations in Fig. 4, using the slope value from Fig. 3C in which a distributed flash photorelease of IP_3 evoked first puffs at a rate (inverse mean latency) of 1.11 s^{-1} per second of flash duration. The heat maps of the predicted puff-triggering rates for IP_3 diffusion coefficients of 10 and 280 $\mu m^2 s^{-1}$ showed different probability patterns (Fig. 5A, B). From these simulation results, we derived the corresponding probabilities of observing an initial puff at selected distances along the

Author Manuscript Author Manuscript Author Manuscript Author Manuscript

modeled cell as a function of time, taking into account the increasing chance that a puff would have already occurred during prior time points (Figs. 5C, D). Finally, we computed how the first-puff latencies varied with distance from the spot where IP3 was introduced (the simulated spot flash stimulation) for a 500 ms spot flash duration and respective diffusion coefficients of 10 and 280 $\mu m^2 s^{-1}$ (Figs. 5E, F, blue curves).

In the case of the 280 $\mu m^2 s^{-1}$ diffusion coefficient, almost all first puffs were predicted to arise within 5 s of the introduction of IP_3 (Fig. 5D) and there was only a small dependence of first-puff latencies on distance from the introduction spot; increasing from about 1.5 s at the introduction site to about 2.5 s at the far end of the modeled cell (Fig. 5F). Indeed, those predicted values are close to the experimental measurements obtained with distributed flash stimulation across the cell (indicated by the red line in Fig. 5F), concordant with a rapid spatial equilibration of IP_3. In marked contrast, simulations with a diffusion coefficient of 10 $\mu m^2 s^{-1}$ showed large differences in puff-latency distributions with distance (Fig. 5C). Mean latencies near the IP_3 introduction site (~ 0.4 s) were shorter than following distributed introduction of the same amount of IP_3 (red line), whereas they lengthened to ~11 s at the end of the modeled cell farthest from the site of IP_3 introduction (Fig. 5E).

Estimating the IP_3 diffusion coefficient by fitting simulated to experimental data

The simulation results indicated that a diffusion coefficient of 10 $\mu m^2 s^{-1}$ better matched our experimental results than with a diffusion coefficient of 280 $\mu m^2 s^{-1}$. To refine our estimate of the IP_3 diffusion coefficient, we performed additional simulations using a range of diffusion coefficients between 1 and 280 $\mu m^2 s^{-1}$. Simulations were performed by calculating the probabilities of puff occurrence within 30 s of introduction of IP_3 (mimicking experimental recording time for the response to spot flash stimulation of i-IP_3). This procedure normalizes the comparison between experimental and simulated data, by accounting for missed long-latency puffs that may have occurred after the end of recordings (see methods S1).

Superimposition of the experimental data corresponding to spot flash stimulation for 500 ms (Fig. 2B) with the predicted mean first-puff latencies as a function of distance from a 500 ms duration introduction of IP_3 showed that the experimental data matched best with the simulation curves generated with diffusion constants of 5 or 10 $\mu m^2 s^{-1}$ (Fig. 6A). Plotting the experimental data together with simulation curves for all flash durations further indicated that a diffusion coefficient of 280 $\mu m^2 s^{-1}$ did not match the data well (Fig. S5). We quantified the goodness of fit to the simulated relationships by calculating the mean squared differences between experimental and simulated data for different values of IP_3 diffusion coefficients (Fig. 6B). For each flash duration, and for each selected diffusion coefficient, the mean squared error is the average of the squared differences between the binned mean observed latencies (Fig. 6A and Fig. S5) and the predicted mean latencies at the corresponding distances. This analysis showed that the minimum values (representing the best fit) were obtained with diffusion coefficients between 3 and 10 $\mu m^2 s^{-1}$, with the best-fit diffusion coefficient tending to higher values with increasing flash duration.

We did not apply this model to estimate a diffusion coefficient for IP_3 in COS-7 cells because their more complex morphology cannot be approximated as a one-dimensional

Author Manuscript Author Manuscript Author Manuscript Author Manuscript

situation. Nevertheless, the observed ~3-fold lengthening of mean puff latency over a distance of 20 μm from the site of spot flash stimulation indicates that diffusion of IP_3 is strongly hindered in COS-7 cells (Fig. S3B). If IP_3 were to diffuse freely with a diffusion coefficient of 280 $\mu m^2\ s^{-1}$, its concentration would equilibrate over this distance within <1s, so puff latencies would show little or no apparent dependence on distance.

Range of action of IP_3

Allbritton *et al.* (1) defined the range of action of a messenger as

$$\sqrt{2D\tau} \quad \text{Eq. 1}$$

where D is the effective diffusion coefficient of the messenger and τ is its mean lifetime before degradation. That expression represents an equilibrium value and does not take into account the time it takes a messenger to diffuse from a localized source. In light of our observations of slow diffusion of IP3, we propose a re-definition of the range of action as (see methods S2: Range of action calculation)

$$\text{range of action} = \frac{\int_0^\infty x\Phi_T(x)dx}{\Phi_T(x)dx} \quad \text{Eq. 2}$$

$$\Phi_T(x) \overset{\text{def}}{=} \int_0^T [IP_3]_{D,\tau}(x,t)dt \quad \text{Eq. 3}$$

where x is the distance from the IP_3 source, T is any given time, t, after deposition of messenger, and $[IP_3]_{D,\tau}(x,t)$ is the IP_3 concentration that results from diffusion with effective coefficient, D, and mean life time, τ. Intuitively, this can be considered as the distance from a point source over which one half of the total cumulative actions of the messenger would have occurred (Figs. 7A, B). Our definition also corresponds to the median distance over which a messenger that is continuously deposited in the cell at position x = 0 is spread when a time T has elapsed since the deposition was initiated (16). Heat maps illustrate the range of action predicted by Eq. 2 as a function of effective diffusion coefficient and degradation rate, calculated for 0.1, 1, 10 and 100 s following an instantaneous appearance of the messenger (Fig. 7C–F). These heat maps showed that the range of action over short intervals (≤ 1s) is narrowly restricted (<5 μm) and dominated by the diffusion coefficient (Fig. 7C,D), whereas at longer intervals the range of action becomes more extended and is dependent on both the diffusion coefficient and rate of degradation of the messenger (Fig. 7E,F).

Author Manuscript Author Manuscript Author Manuscript Author Manuscript

DISCUSSION

Intracellular diffusion and range of action of IP_3

We investigated the diffusion of IP_3 in neuroblastoma cells by locally photoreleasing a poorly-metabolized IP_3 analog at one end of these elongated cells and monitoring its subsequent spread by the timing of discrete IP_3-evoked, Ca^{2+}-release events (puffs) at multiple sites along the cell. Using first-puff latency as an endogenous reporter of local [IP_3], we obtained estimates of the effective diffusion coefficient of IP_3 in the cytoplasm of intact mammalian cells under physiologically relevant IP_3 concentrations, with minimal perturbation of cellular function and structure.

By comparing our experimental puff latency data to predicted puff triggering probabilities in a 1-dimensional model, we obtained best agreement for an effective diffusion coefficient D for IP_3 ~ 3–10 $\mu m^2\ s^{-1}$. Although our model does not fully replicate the complex 3-dimensional cellular architecture, we selected relatively elongated cells for study. Another possible source of error is that basal Ca^{2+} concentrations were not fully clamped by the EGTA loaded into the cells, so that puff triggering may have been accelerated by a slow, progressive increase in basal free cytosolic [Ca^{2+}] (Fig. 1C). This increase in basal [Ca^{2+}] would have the most pronounced effect at sites distant from the photolysis spot where puff latencies were long, with any potential net effect that our values of for the IP_3 diffusion coefficient are overestimated.

The effective diffusion coefficient of IP_3 that we determined is ~30 fold slower than the value (283 ± 53 $\mu m^2\ s^{-1}$) reported by Allbritton *et al.* (1). The larger value has become widely accepted (17–20), leading to the conclusion that the range of action of IP_3 is sufficiently large that it functions as a global messenger in mammalian cells of typical size (1,2). Published values for the half-life (τ) of IP_3 in cells range widely from one to several seconds in mammalian cells (2), including 10 or 20 s in neuroblastoma cells (11, 21) to a minute or more in *Xenopus* oocytes (2, 21). Defining the range of action as in Eq. 1, and assuming D = 280 $\mu m^2\ s^{-1}$ and τ = 1 s, Allbritton *et al.* (1) obtained a range of action of about 25 μm. However, taking our value of the effective diffusion coefficient D = 3–10 $\mu m^2\ s^{-1}$ the range reduces to < 5 μm, indicating that IP_3 should no longer be considered a ‘global’ messenger, but that appreciable spatial gradients of IP_3 may arise within even small cells. Indeed the range of action of IP_3 is comparable to that (~5 μm) for the buffered diffusion of Ca^{2+} (1, 13), which is considered a local messenger.

Physiological implications of hindered diffusion of IP_3

The restricted effective diffusion of IP_3 likely has important physiological implications for IP_3-mediated signaling. Ca^{2+} release from the endoplasmic reticulum (ER) through IP_3Rs requires binding of both cytosolic IP_3 and Ca^{2+} to receptor sites on the tetrameric IP_3R, leading to a regenerative process of Ca^{2+}-induced Ca^{2+} release (22). This process can support the generation of propagating Ca^{2+} waves by a fire-diffuse-fire model (23), wherein Ca^{2+} released through IP_3Rs at one site diffuses to activate release through surrounding IP_3-bound IP_3Rs. Thus, although Ca^{2+} wave propagation can be considered to overcome the limited effective diffusional range of Ca^{2+} ions, the extent to which a Ca^{2+} wave can

Author Manuscript Author Manuscript Author Manuscript Author Manuscript

propagate is set by the diffusional spread of IP_3, if IP_3 is generated from a localized source. The impact of the diffusional spread will be particularly strong in extended cellular processes, such as neuronal dendrites, and in the propagation of intercellular Ca^{2+} signals mediated by diffusion of IP_3 through gap junctions (24, 25).

The expression (Eq. 1) for the range of action as formulated by Allbritton *et al.* (1) does not adequately describe many physiological situations. If the messenger is not degraded, its range of action goes to infinity. Furthermore, the range of action given by Eq. 1 does not take time into account. Our data provide a clear example of these limitations, in that Ca^{2+} signals at the distal end of the cell arose after latencies ~ 10 fold longer than near the site of photoreleased IP_3, even though degradation of i-IP_3 was negligible (11). Timing is crucial for many physiological processes - it is not merely the final concentration to which a diffusible messenger ultimately increases, but how quickly it increases and subsequently decreases that are also critical for shaping the cellular response to the messenger. In place of the Allbritton *et al.* expression, we thus propose a more biologically relevant expression (Eq. 2), equating the range of action as the distance from the source over which one half of the total cumulative actions of the messenger would have occurred at any given time (Fig. 7A) (methods S2: Range of action calculation). Using our expression for range of action, at long times ($t \gg \tau$) after the appearance of the messenger, the expression converges to $\sqrt{D\tau}$, which yields a range of action shorter by a factor of $\sqrt{2}$ than that given by the Allbritton *et al.* expression. For example, for D = 10 $\mu m^2 s^{-1}$ and τ = 1 s, the steady-state range of actions given by the different expressions are, respectively, about 3.3 and 4.5 μm. Potentially of more biological importance, Eq. 2 indicates that for short times ($t < \tau$) the range of action becomes increasingly independent of messenger degradation and varies approximately as a square root function of time. Considering the same example, the predicted range of action further reduces to 1.60 μm over an interval of 500 ms following introduction of messenger.

This dependence on IP_3 metabolism may be of particular importance for IP_3 signaling in neurons, where the dual gating of IP_3 receptors by IP_3 and cytosolic Ca^{2+} has been proposed to function as a coincidence detector. Specifically, the ability of IP_3 to evoke intracellular Ca^{2+} release as it diffuses along a dendrite after local metabotropic receptor activation at one site may be promoted by a subsequent action potential that evokes entry of Ca^{2+} through plasma membrane channels (26, 27), or by summation with local production of IP_3 (28) at other sites further along the dendrite. A lower effective diffusion coefficient of IP_3 would narrow the spatiotemporal window over which the coincidence of these signals would occur, because the spread of IP_3 would be more restricted and IP_3 concentrations at distant sites may rise too slowly to coincide with the increase in Ca^{2+}.

Hindered diffusion of IP_3 by binding to 'silent' IP_3Rs

What might underlie the markedly hindered diffusion of IP_3 in neuroblastoma cells, and why does this differ so markedly from the free mobility of IP_3 reported by Allbritton *et al.* in oocyte cytoplasmic extracts? The slow intracellular diffusion of IP_3 in the cytosol cannot readily be explained by nonspecific factors, such as tortuosity or viscosity, given that the diffusion coefficient of ATP – a molecule of similar size and identical charge to IP_3 – is only slightly lower in cells than in free solution (respectively, 248 and 349 $\mu m^2 s^{-1}$ (29)). Instead,

Author Manuscript Author Manuscript Author Manuscript Author Manuscript

we propose that diffusion of IP_3 is limited by binding to the large number of IP_3Rs estimated to be present in SH-SY5Y and other mammalian cells (5). The motility of IP_3Rs in the ER membrane is low with a diffusion coefficient <0.1 $\mu m^2 s^{-1}$ (6), so they can be considered as immobile on the time and distance scales of our experiments. Binding to stationary, unoccupied receptor sites is thus expected to slow the effective diffusion of IP_3 in a manner analogous to the slowing of diffusion of Ca^{2+} ions by binding to immobile cytoplasmic buffers. The ability of IP_3Rs to buffer IP_3 and slow its effective diffusion will diminish at increasing concentrations of IP_3 as an increasing fraction of the binding sites becomes occupied. Indeed, our results showed a trend for the effective diffusion coefficient to increase from about 3 to 10 $\mu m^2 s^{-1}$ over the 5-fold range of photoreleased i-IP_3 that we explored. We anticipate that the i-IP_3 released represents a physiological range of IP_3 concentrations, because even the weakest photolysis flash evoked robust global Ca^{2+} waves in cells not loaded with EGTA (Fig. S2).

Concordant with a mechanism of physiological IP_3 buffering, Finch and Augustine observed that Ca^{2+} signals evoked by spot photorelease of IP_3 (not the poorly metabolized i-IP_3 analog) in the dendrites of cerebellar Purkinje cells were restricted to a few micrometers, a finding that they interpreted to result from binding to the high density of IP_3Rs in these cells (30). In contrast, the experiments of Allbritton *et al.* (1) were made using cytosolic extracts from *Xenopus* oocytes in which IP_3Rs are concentrated in a thin circumferential shell around these giant cells (31, 32). The concentration of IP_3Rs in these extracts would have been diluted by the large bulk of cytoplasm from the oocyte interior. Moreover, binding to receptor sites may have been saturated by the concentration of radiolabelled IP_3 (100 nM total IP_3) applied to monitor diffusion. In this context, we therefore believe the *Xenopus* oocyte cytoplasm does not serve well as a model system for small mammalian cells.

The calculated diffusion coefficient for IP_3 in a medium with twice the viscosity of water is about 250 $\mu m^2 s^{-1}$ (1), similar to the measured value for ATP in cells (29). We interpret our finding of an effective diffusion coefficient of ≤ 10 $\mu m^2 s^{-1}$ as arising because specific binding of IP_3 to immobile sites slows its effective diffusion by a factor of ≥25. Assuming that binding equilibrates rapidly and that only a small fraction of all sites are bound, the effective diffusion coefficient D_{eff} is given by:

$$D_{eff} = \frac{D}{1+R} \quad \text{Eq. 4}$$

where D is the diffusion coefficient in the absence of binding and R is the ratio of concentration of binding sites to the dissociation constant K_D of binding to these sites (33). Our results thus lead to a value of R ≥24. This differs markedly from the value of ~1 that is calculated from the intracellular IP_3R concentration of 100 nM and K_D of 113 nM reported by Taylor's group (5, 34). With an R of 1, the effective diffusion coefficient of IP_3 would be reduced by no more than a factor of two from that in the absence of binding.

Silent and functional IP_3Rs

Ca^{2+} puffs involve the concerted opening of several IP_3Rs, tightly clustered at immobile, sparsely distributed sites throughout the cell (3, 4). A long-standing question is why Ca^{2+}

Author Manuscript Author Manuscript Author Manuscript Author Manuscript

release is restricted to these specific sites, involving only about 3% of the total number of IP_3Rs in the cell, whereas the great majority of IP_3Rs appear functionally 'silent' under the same conditions even though the slow diffusion of IP_3 suggests that they bind IP_3 (5, 35).

Our results, considered together with evidence that the tetrameric IP_3R channel requires IP_3 to be bound to all four receptor sites before it can be activated (5, 36), cast light on this issue. The hindered diffusion of IP_3, and relative insensitivity of the effective diffusion coefficient to changes in amount of photoreleased IP_3 (from ~3 $\mu m^2 s^{-1}$ with a 100 ms flash to ~ 10 $\mu m^2 s^{-1}$ with a 500 ms flash), indicated that a substantial fraction of binding sites must remain unoccupied. How then can Ca^{2+} puffs be generated under these conditions, given that they involve the concerted opening of several, tightly clustered IP_3Rs (3, 4)? As an example, for a cluster of four channels, the probability that all will be available to open during a puff increases as the 16^{th} power of $[IP_3]$, so a concentration that yields a 50% probability that all four IP_3Rs are activated (binding four IP_3 molecules) corresponds to an overall occupancy of receptor sites of 95.8%. It seems that the IP_3Rs active at puff sites must be functionally different from the 'silent' receptors that hinder binding, in addition to their differing spatial localization and motility (5, 6, 35). The mechanism remains unknown, but possibilities include that receptors at puff sites exhibit a much higher affinity of IP_3 binding, or that their gating properties are modified so that channel opening requires binding of fewer than four IP_3 molecules per tetramer.

MATERIALS AND METHODS

Reagents

Unless otherwise indicated all reagents were obtained from Sigma and cell culture media from Invitrogen, Carlsbad, CA

Cell Culture

SH-SY5Y human neuroblastoma cells were cultured as previously described (4) in a 1:1 mix of Ham's F12 medium and Eagle MEM, supplemented with fetal calf serum (10%, v/v) and nonessential amino acids (1% v/v). Cells were incubated at 37°C in a humidified incubator with 95% air and 5% CO_2 and were passaged every 2–3 days to a maximum of 20 passages. Four days prior to imaging, cells were harvested in Ca^{2+}/Mg^{2+}-free phosphate-buffered saline and cultured on glass coverslips in Petri dishes (35mm dish, No. 1.0 coverglass; MatTek, Ashland, MA) at a density of ~3×10^4 cells/mL. On the day of imaging, cells were washed into HEPES-buffered saline solution (HBS, composition in mM: NaCl, 135; KCl, 5; MgCl, 1.2; $CaCl_2$, 2.5; Hepes 5; glucose, 10; pH 7.4)

Ca^{2+} imaging and localized photorelease of i-IP_3

Cultured SH-SY5Y cells were loaded for imaging by incubation with membrane-permeant esters of Fluo-4 (1 μM, Invitrogen), EGTA (5 μM, Invitrogen), and caged i-IP_3 (ci-IP_3, 1 μM, SiChem, Bremen, Germany) in HBS, as described (4). Cells averaged about 40 μm in length along the cell body (Fig. S4A). Cytosolic Ca^{2+} changes were imaged using a TIRF microscope system (4) constructed around an Olympus IX 70 microscope with a 60× TIRF objective (NA, 1.45). Fluo-4 fluorescence was excited by 488 nm laser light within an

Author Manuscript Author Manuscript Author Manuscript Author Manuscript

evanescent field extending a few hundred nanometers into the cells, and emitted fluorescence (λ > 510 nm) was imaged at a resolution of 256 × 256 pixels (1 pixel = 0.266 μm) at an exposure time of 15 ms (~66 frames sec^{-1}) using the center quad of an Evolve 512 electron-multiplied CCD camera (Roper Scientific; Tucson, AZ). Image data were acquired as stack files using MetaMorph v7.7 (Universal Imaging/Molecular Devices; Sunnyvale, CA) and were analyzed offline to detect the locations of puff sites and measure puff latencies. The custom software used for analysis is described in (14), and is freely available on request to the authors of that paper. Measurements were exported to Microcal Origin V. 8.0 (OriginLab, Northampton, MA) for analysis and graphing. Unless otherwise noted, data are presented as means ± 1 S.E.M.

Photorelease of i-IP_3

Photolysis of ci-IP_3 was evoked by a custom-built system using computer- controlled galvanometer mirrors to direct light from a 405 nm laser diode module. The laser light was focused to a spot in the specimen (Fig. S4B), which could be steered to any desired location within the imaging field using dim light from a coaxial 450 nm laser as a ‘guide star’ to excite fluorescence in Fluo-4-loaded cells without causing photorelease of i-IP_3. A computer-generated TTL signal controlled the duration of the 405 nm photolysis spot flash, and a variable neutral density filter wheel controlled its intensity. Experiments were performed using photolysis flashes of given duration and fixed intensity; either with the laser spot remaining stationary at one end of a cell to evoke localized photorelease of i-IP_3 (spot flash), or scanned along the length of a cell during the same flash duration to evoke a spatially distributed photorelease (distributed flash). In the latter case, a line was defined by clicking the computer mouse after positioning the guide laser spot at each end of the cell, and the computer then stepped the 405 nm laser spot in 10 equal increments along the line during the flash duration. For example, a 100 ms flash would be delivered as 10 exposures, each of 10 ms duration, spaced at 4 μm increments along a cell 40 μm in length. Given that flash durations were short (100–500 ms) in comparison to puff latencies this distributed flash protocol leads to an approximately uniform photorelease of i-IP_3 throughout the cell, in an amount equivalent to that photoreleased by a stationary spot flash of the same duration and intensity.

Analytical derivation and numerical simulation of puff latencies

To simulate the diffusion of IP_3 and subsequent triggering of initial puffs following spot flash stimulation, we applied a simplified one-dimensional model. Analytical solutions of the model are presented in the methods S1. To generate model data with which to fit to experimental observations, we performed numerical simulations of these solutions. The cell was represented as an array 40 μm long, with closed ends, comprised of 100 elements each containing a single puff site. To simulate uncaging of IP_3, we increased the concentration of IP_3 a fixed amount every time step during the duration of the photolysis flash. The spatial profile of uncaging was simulated as a Gaussian curve with a width (σ = 1.35 um) corresponding to that of the UV laser spot. Because i-IP_3 is metabolically degraded more slowly than endogenous IP_3, the rate of metabolism was set to zero except where otherwise noted; that is to say, the total amount of IP_3 remained constant after the uncaging period. To then simulate the probability of a puff being triggered at each spatial element, we assumed a

Author Manuscript Author Manuscript Author Manuscript Author Manuscript

linear relationship between [IP_3] and puff triggering (10), with a rate constant (1.11 s^{-1} per 1 s flash duration) derived from experiments (Fig. 3C) in which corresponding amounts of i-IP_3 were photoreleased uniformly throughout cells by the distributed flash protocol. For each spatial element, we then took the triggering rate as given by the concentration of IP_3 at a given time step and calculated the probability of observing the first puff at that site over successive time steps. Simulations were terminated after 30 s to match the duration of experimental recordings, and calculations of mean first-puff latencies were made only over this interval. Thus, mean values from both experimental and simulated data were unaffected by 'missed' sites that failed to show a puff within 30s.

Supplementary Material

Refer to Web version on PubMed Central for supplementary material.

Acknowledgments

We thank Nick Hengartner and David Colquhoun for helpful discussions and Brett Settle for help with software development. **Funding:** This work was supported by the NIH through grants R37 GM 048071 (to I.P.), RO1 GM 065830 (to J.E.P. & I.P.) and F31 GM 119330-01 (to K.E.); and by UBA and FONCyT (Argentina) through grants UBACyT 20020130100480BA and PICT 2013-1301 (to SD).

REFERENCES AND NOTES

1. Allbritton NL, Meyer T, Stryer L. Range of messenger action of calcium ion and inositol 1,4,5-trisphosphate. Science. 1992; 258:1812–1815. [PubMed: 1465619]
2. Sims CE, Allbritton NL. Metabolism of inositol 1, 4, 5-trisphosphate and inositol 1, 3, 4, 5-tetrakisphosphate by the oocytes of *Xenopus laevis*. J Biol Chem. 1998; 273:4052–4058. [PubMed: 9461597]
3. Smith IF, Wiltgen SM, Shuai J, Parker I. Ca^{2+} puffs originate from preestablished stable clusters of inositol trisphosphate receptors. Sci Signal. 2009; 2:ra77. [PubMed: 19934435]
4. Smith IF, Parker I. Imaging the quantal substructure of single IP_3R channel activity during Ca^{2+} puffs in intact mammalian cells. Proc Natl Acad Sci U S A. 2009; 106:6404–6409. [PubMed: 19332787]
5. Taylor CW, Konieczny V. IP_3 receptors: Take four IP_3 to open. Sci Signal. 2016; 9:2–6.
6. Smith IF, Swaminathan D, Dickinson GD, Parker I. Single-molecule tracking of inositol trisphosphate receptors reveals different motilities and distributions. Biophys J. 2014; 107:834–845. [PubMed: 25140418]
7. Wilson BS, Pfeiffer JR, Smith AJ, Oliver JM, Oberdorf JA, Wojcikiewicz RJ. Calcium-dependent clustering of inositol 1,4,5-trisphosphate receptors. Mol Biol Cell. 1998; 9:1465–1478. [PubMed: 9614187]
8. Tovey SC, De Smet P, Lipp P, Thomas D, Young KW, Missiaen L, De Smedt H, Parys JB, Berridge MJ, Thuring J, Holmes A, Bootman MD. Calcium puffs are generic $InsP_3$-activated elementary calcium signals and are downregulated by prolonged hormonal stimulation to inhibit cellular calcium responses. J Cell Sci. 2001; 114:3979–3989. [PubMed: 11739630]
9. CJ, Yao PIY. Quantal puffs of intracellular Ca^{2+} evoked by inositol trisphosphate in *Xenopus* oocytes. J Physiol. 1995; 482:533–553. [PubMed: 7738847]
10. Dickinson GD, Swaminathan D, Parker I. The probability of triggering calcium puffs is linearly related to the number of inositol trisphosphate receptors in a cluster. Biophys J. 2012; 102:1826–1836. [PubMed: 22768938]
11. Dakin K, Li WH. Cell membrane permeable esters of d-myo-inositol 1,4,5-trisphosphate. Cell Calcium. 2007; 42:291–301. [PubMed: 17307252]

Author Manuscript Author Manuscript Author Manuscript Author Manuscript

12. Smith IF, Wiltgen SM, Parker I. Localization of puff sites adjacent to the plasma membrane; functional and spatial characterization of Ca^{2+} signaling in SH-SY5Y cells utilizing membrane-permeant caged IP_3. Cell Calcium. 2010; 45:65–76.
13. Dargan SL, Parker I. Buffer kinetics shape the spatiotemporal patterns of IP_3 -evoked Ca^{2+} signals. J Physiol. 2003; 553:775–788. [PubMed: 14555715]
14. Ellefsen KL, Settle B, Parker I, Smith IF. An algorithm for automated detection, localization and measurement of local calcium signals from camera-based imaging. Cell Calcium. 2014; 56:147–56. [PubMed: 25047761]
15. Parker I, Yao Y, Ilyin V. Fast kinetics of calcium liberation induced in *Xenopus* oocytes by photoreleased inositol trisphosphate. Biophys J. 1996; 70:222–37. [PubMed: 8770200]
16. Bergmann S, Sandler O, Sberro H, Shnider S, Schejter E, Shilo BZ, Naama B. Pre-steady-state decoding of the bicoid morphogen gradient. PLoS Biol. 2007; 5:0232–0242.
17. Decrock E, De Bock M, Wang N, Gadicherla AK, Bol M, Delvaeye T, Vandenabeele P, Vinken M, Bultynck G, Krysko DV, Leybaert L. IP_3, a small molecule with a powerful message. Biochim Biophys Acta - Mol Cell Res. 2013; 1833:1772–1786.
18. Gelens L, Anderson GA, Ferrell JE. Spatial trigger waves: positive feedback gets you a long way. Mol Biol Cell. 2014; 25:3486–93. [PubMed: 25368427]
19. Konieczny V, Keebler MV, Taylor CW. Spatial organization of intracellular Ca^{2+} signals. Semin Cell Dev Biol. 2012; 23:172–180. [PubMed: 21925615]
20. Kruse M, Vivas O, Traynor-Kaplan A, Hille B. Dynamics of phosphoinositide-dependent signaling in sympathetic neurons. J Neurosci. 2016; 36:1386–1400. [PubMed: 26818524]
21. Wang SS, Alousi AA, Thompson SH. The lifetime of inositol 1,4,5-trisphosphate in single cells. J Gen Physiol. 1995; 105:149–71. [PubMed: 7730788]
22. Foskett JK, White C, Cheung K, Mak DD. Inositol trisphosphate receptor Ca^{2+} release channels. Physiol Rev. 2007; 87:593–658. [PubMed: 17429043]
23. Dawson SP, Keizer J, Pearson JE. Fire-diffuse-fire model of dynamics of intracellular calcium waves. Proc Natl Acad Sci U S A. 1999; 96:6060–6063. [PubMed: 10339541]
24. Leybaert L, Sanderson MJ. Intercellular Ca^{2+} waves: mechanisms and function. Physiol Rev. 2012; 92:1359–92. [PubMed: 22811430]
25. Lock JT, Parker I, Smith IF. Communication of Ca^{2+} signals via tunneling membrane nanotubes is mediated by transmission of inositol trisphosphate through gap junctions. Cell Calcium. 2016; doi: 10.1016/j.ceca.2016.06.004
26. Manita S, Ross WN. IP_3 mobilization and diffusion determine the timing window of Ca^{2+} release by synaptic stimulation and a spike in rat CA1 pyramidal cells. Hippocampus. 2010; 20:524–539. [PubMed: 19475649]
27. Ross WN. Understanding calcium waves and sparks in central neurons. Nat Rev Neurosci. 2012; 13:157–168. [PubMed: 22314443]
28. Reissner KJ, Pu L, Schaffhausen JH, Boyle HD, Smith IF, Parker I, Carew TJ. A novel postsynaptic mechanism for heterosynaptic sharing of short-term plasticity. J Neurosci. 2010; 30:8797–8806. [PubMed: 20592201]
29. Hubley MJ, Rosanske RC, Moerland TS. Diffusion-coefficients of ATP and creatine-phosphate in isolated muscle - pulsed gradient P-31 NMR of small biological samples. NMR Biomed. 1995; 8:72–78. [PubMed: 7547189]
30. Finch EA, Augustine GJ. Local calcium signalling by inositol-1,4,5-trisphosphate in Purkinje cell dendrites. Nature. 1998; 396:753–756. [PubMed: 9874372]
31. Callamaras N, Parker I. Inositol 1,4,5-trisphosphate receptors in *Xenopus laevis* oocytes: Localization and modulation by Ca^{2+} Cell Calcium. 1994; 15:66–78. [PubMed: 8149406]
32. Kume S, Muto A, Aruga J, Nakagawa T, Michikawa T, Furuichi T, Nakade S, Okano H, Mikoshiba K. The *Xenopus* IP_3 receptor: Structure, function, and localization in oocytes and eggs. Cell. 1993; 73:555–570. [PubMed: 8387895]
33. Crank, J. The mathematics of diffusion. 2. Oxford University Press; 1979.
34. Ding Z, Rossi AM, Riley AM, Rahman T, Potter BVL, Taylor CW. Binding of inositol 1, 4, 5-trisphosphate (IP_3) and Adenophostin A to the N-terminal region of the IP_3 receptor:

Author Manuscript Author Manuscript Author Manuscript Author Manuscript

Thermodynamic analysis using fluorescence polarization with a novel IP_3 receptor ligand. Mol Pharmacol. 2010; 77:995–1004. [PubMed: 20215561]

35. Parker I, Smith IF. Recording single-channel activity of inositol trisphosphate receptors in intact cells with a microscope, not a patch clamp. J Gen Physiol. 2010; 136:119–127. [PubMed: 20660654]
36. Alzayady KJ, Wang L, Chandrasekhar R, LEW, Van Petegem F, Yule DI. Defining the stoichiometry of inositol 1,4,5-trisphosphate binding required to initiate Ca^{2+} release. Sci Signal. 2016; 9:1–13.
37. Keener, J., Sneyd, J. Mathematical Physiology. Springer New York; New York, NY: 2009. vol. 1 of *Interdisciplinary Applied Mathematics*

Author Manuscript Author Manuscript Author Manuscript Author Manuscript

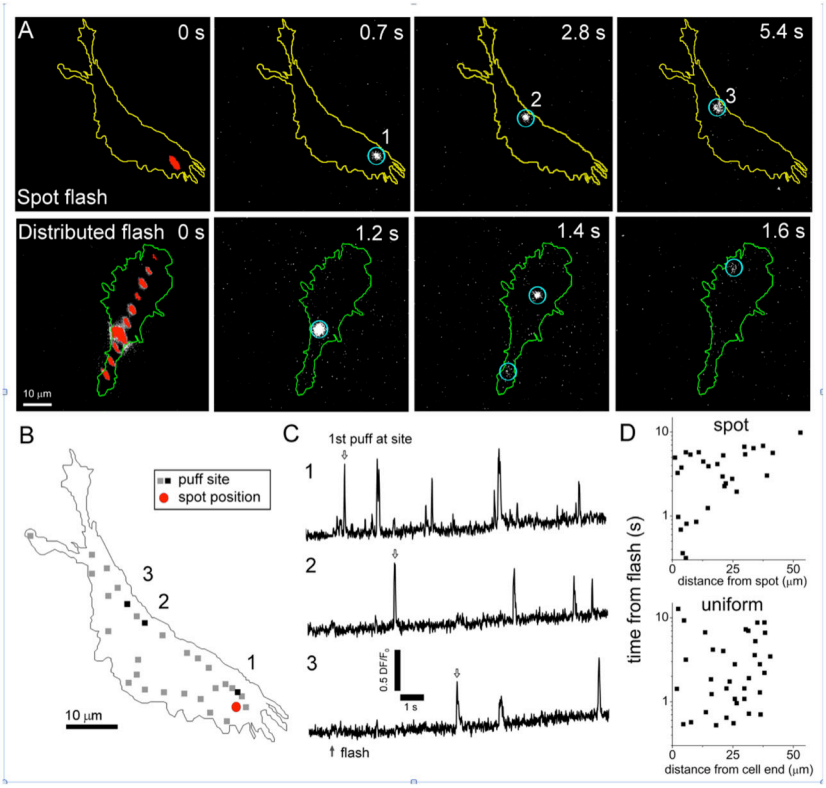

Fig. 1. Latencies of Ca^{2+} puffs evoked by localized and distributed laser spot photorelease of i-IP_3

(A) The top row of panels shows the location of a stationary laser spot flash (200 ms duration) delivered to an SH-SY5Y cell at time zero (red spot, left panel), and image frames at different times following the flash showing the first puffs arising at selected locations (circled). Fluorescence of Fluo-4 during puffs is depicted on an arbitrary grey scale. The bottom row of panels shows corresponding images in a different cell, where a laser flash of the same intensity and total duration was distributed as 10 individual spots spaced evenly along the length of the cell. Scale bar, 10 µm. (**B**) Map of the same cell as in the top row of (A), showing the locations of the puffs numbered in (A) as black squares, the locations of all other identified puff sites marked as grey squares, and the location of the stationary laser spot marked by the red circle. Scale bar, 10 µm. (**C**) Representative traces showing Ca^{2+}-dependent fluorescence ratio changes ($\Delta F/F_0$) measured from small regions of interest (1.3 × 1.3 µm) centered on the puff sites numbered in (A) and (B). The black arrow indicates the time of the spot flash; open arrows mark times of the first puff at each site. (**D**) Scatter plots show measurements of first-puff latencies from all sites in the two cells illustrated in (A) as a function of the distance of that site from the stationary spot flash (top) or from the lower end of the cell in the case of the distributed flash (bottom). Latencies are plotted on a logarithmic scale to better encompass the wide range of values.

Author Manuscript Author Manuscript Author Manuscript Author Manuscript

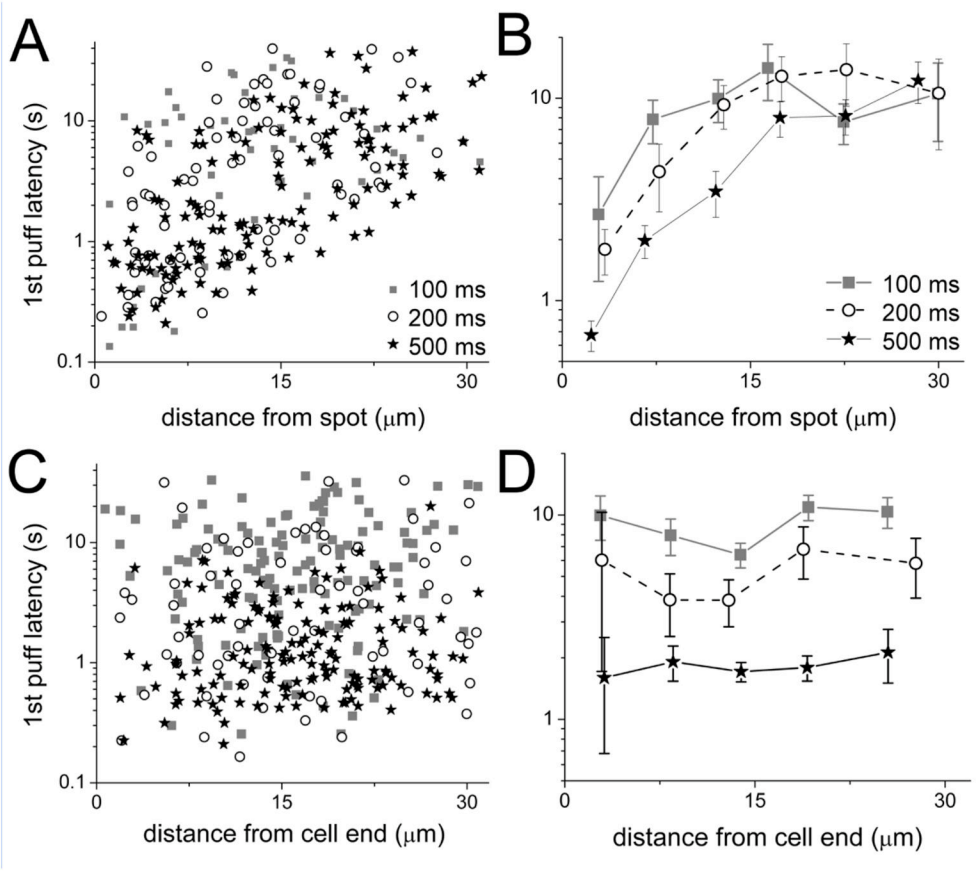

Fig. 2. First-puff latencies increase with increasing distance from spot flash stimulation of i-IP$_3$, but show no systematic variation with position along the cell for distributed flash stimulation of i-IP$_3$

(A) Scatter plot showing first-puff latencies at individual puff sites following spot flash stimulation of i-IP$_3$ as a function of distance from the laser spot following flashes of 100 ms (grey squares; 8 cells, 52 puff sites), 200 ms (open circles; 7 cells, 75 puff sites) and 500 ms duration (stars; 9 cells, 137 puff sites). The y-axis is plotted on a logarithmic scale to better display the wide variability in observed puff latencies. (**B**) Mean measurements of first-puff latency obtained by binning the data in (A) in ~ 5 μm increments. (**C, D**) Corresponding plots of individual (**C**) and mean binned puff latency data (**D**) following distributed flash stimulation of i-IP$_3$. The spot flash intensity and total exposure times were the same as for the spot flash stimulation in (A) and (B). Data from 100, 200, and 500 ms total exposure durations are respectively from 8 cells, 134 puff sites; 8 cells, 76 sites; and 7 cells, 152 sites.

Author Manuscript Author Manuscript Author Manuscript Author Manuscript

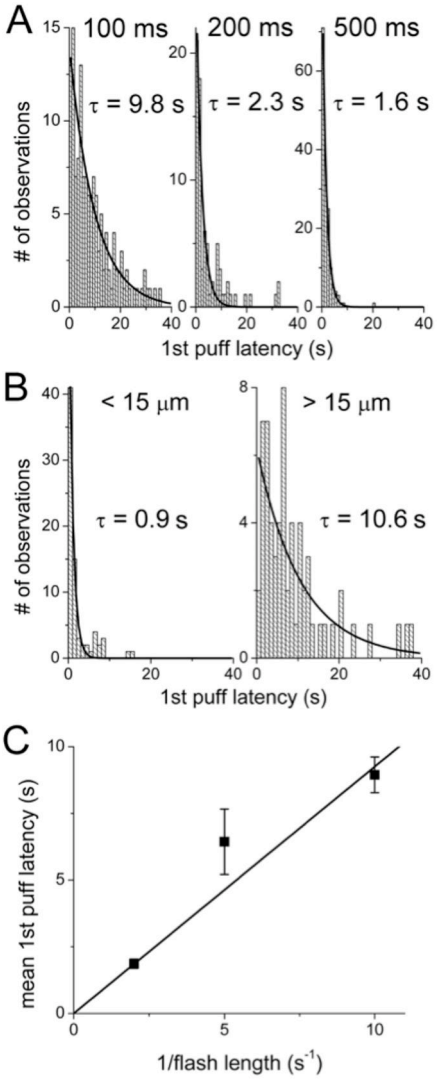

Fig. 3. Distributions of first-puff latencies and dependence of mean first-puff latency on photolysis flash duration

(**A**) Distributions of first-puff latencies evoked following distributed flash stimulation of i-IP_3 with the indicated total flash durations. **(B)** Distributions of first-puff latencies following a 500 ms spot flash stimulation at sites within (left) and beyond (right) 15 μm of the laser spot. Data in (A and B) are fitted by single-exponential functions, with time constants **τ** as indicated. (**C**) Mean first-puff latency following distributed flash stimulation of i-IP_3 plotted as a function of reciprocal flash duration. Error bars indicate + SEM and are smaller than the symbol width for the leftmost point. The data are fitted by a regression line, constrained to the origin, with a slope of 0.90.

Author Manuscript Author Manuscript Author Manuscript Author Manuscript

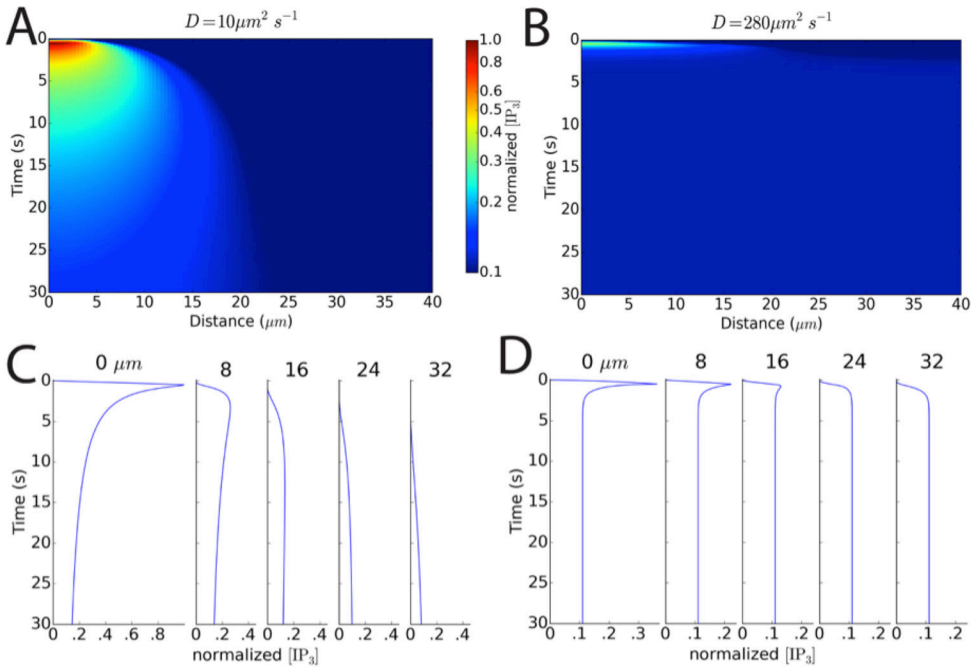

Fig. 4. Simulation of IP_3 diffusion following spot flash stimulation

Panels illustrate the simulated diffusion of IP_3 in a 40 μm long, one-dimensional model of a cell following spot (Gaussian profile with σ = 1.35 μm) flash stimulation at one end with a flash duration of 500 ms. After the flash, the total amount of IP_3 was conserved through cell (no degradation occurred). The diffusion coefficients used in the simulations are indicated at the top. (**A, B)** Heat maps representing IP_3 concentrations at different times (y-axis, with time running from top to bottom) and distances (x-axis) following the beginning of the flash at time zero. IP_3 concentrations are in arbitrary units, but are consistent for both panels. (**C, D**) Temporal profiles of [IP_3] at different distances (indicated in μm) along the modeled cell. Concentrations of IP_3 in both panels are expressed normalized to the peak concentration attained at the photolysis spot site for D = 10 $\mu m^2\ s^{-1}$.

Author Manuscript Author Manuscript Author Manuscript Author Manuscript

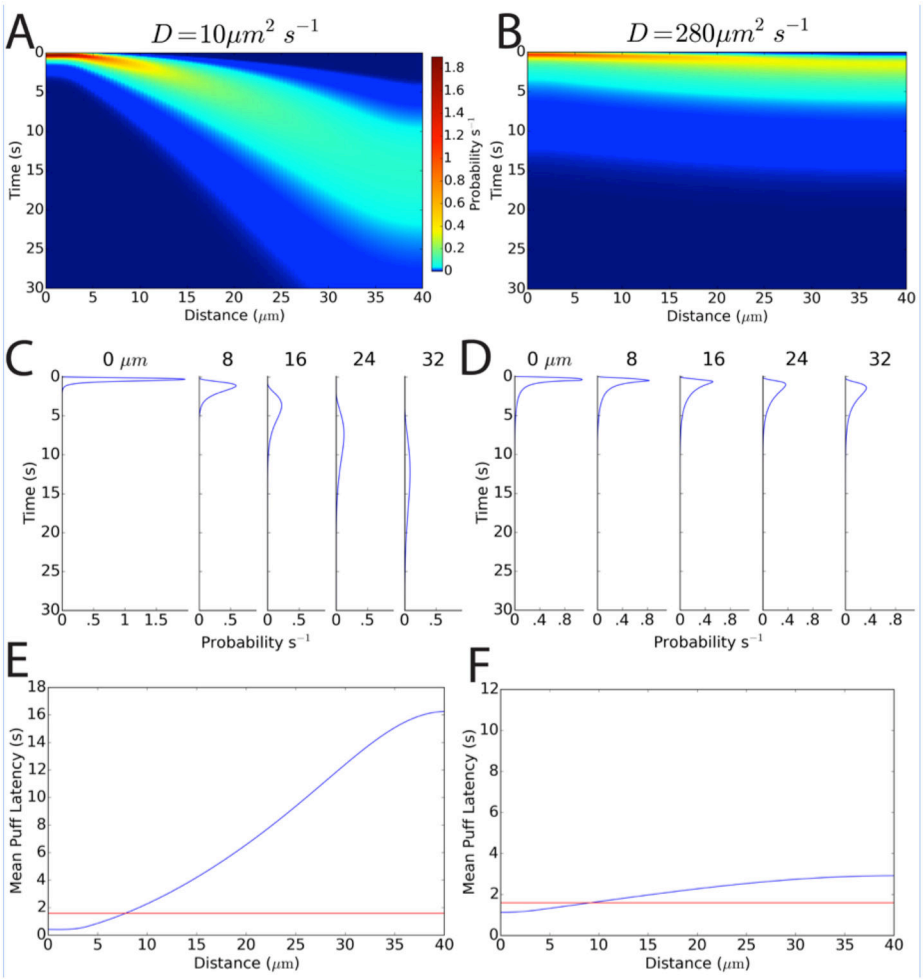

Fig. 5. Simulation of the probability of observing puffs at different times and distances following spot photorelease of IP_3

Simulations were based on the spatiotemporal concentration profiles in Fig. 4, assuming that the probability of puff triggering is a linear function of [IP_3]. The diffusion coefficients used in the simulations are indicated at the top. (**A, B)** Heat maps representing the probability of observing a puff at different times (y-axis, with time running from top to bottom) and distances along the cell (x-axis) following the beginning of the flash at time zero. (**C, D**) Temporal profiles of puff probability at different distances (indicated in μm) along the cell. (**E, F)** Predicted mean latencies of puffs as a function of distance along the cell from the flash. Horizontal lines indicate the mean puff latency if the same total amount of IP_3 were released uniformly along the cell by distributed flash stimulation.

Author Manuscript Author Manuscript Author Manuscript Author Manuscript

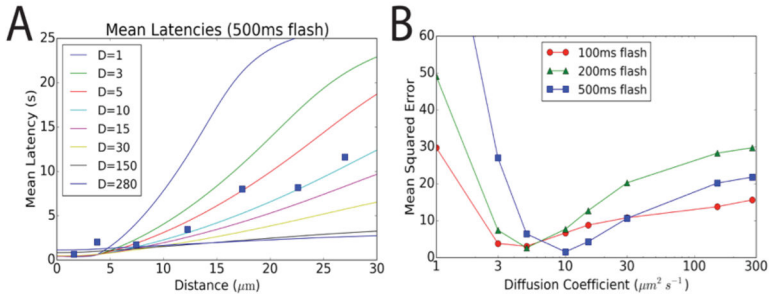

Fig. 6. Comparison of experimental with simulated data indicates an effective intracellular diffusion coefficient for IP_3 of 3–10 $\mu m^2 s^{-1}$

(**A**) Comparison of experimental and predicted first-puff latencies evoked by a 500 ms spot flash stimulation. Curves plot the predicted mean first-puff latencies as a function of distance along the cell from the stationary photolysis spot for various values of IP_3 diffusion coefficient, as indicated in units of $\mu m^2 s^{-1}$. Data points show mean ± SEM of first-puff latencies from the experiment shown in Fig. 2A, B. (**B**) Mean squared error between observed and predicted puff latencies as a function of the simulated IP_3 diffusion coefficient. Curves are shown for experimental and simulated data for flash durations of 100, 200, and 500 ms.

Author Manuscript Author Manuscript Author Manuscript Author Manuscript

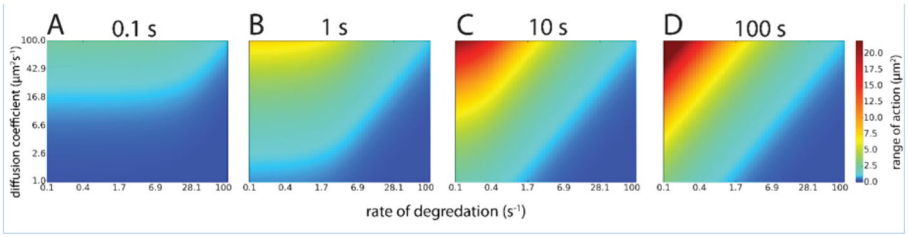

Fig. 7. Time dependence of the range of action of an intracellular messenger

We define the range of action at a given time T as the distance from a transient point source of messenger at which half of its total cumulative actions (given by Eq. 2) will have occurred. (**A, B**) Illustrations showing the range of action after times T = 1 s (A) and T = 10 s (B) for a diffusion coefficient D = 10 $\mu m^2 s^{-1}$ and mean messenger lifetime τ = 10s. The schematic represents a one-dimensional model cell extending infinitely far on each side from a transient, point source of messenger; the profile and range of action are identical for a one-sided model extending infinitely from a closed end where messenger is introduced. The y-axis is in arbitrary units. [**C–F**] Heat maps showing the predicted ranges of action of an intracellular messenger at times T = 0.1 s (**C**), 1 s (**D**), 10 s (**E**), and 100 s (**F**) for different combinations of effective diffusion coefficient and rate of degradation (inverse mean lifetime) of messenger.